Molecular and cytotoxic properties of hIAPP17–29 and rIAPP17–29 fragments: A comparative study with the respective full-length parent polypeptides

ARTICLE *in* EUROPEAN JOURNAL OF MEDICINAL CHEMISTRY · MAY 2014

Impact Factor: 3.45 · DOI: 10.1016/j.ejmech.2014.05.038 · Source: PubMed

7 AUTHORS, INCLUDING:

Francesco Attanasio
Italian National Research Council
35 PUBLICATIONS **182** CITATIONS
SEE PROFILE

Danilo Milardi
Italian National Research Council
76 PUBLICATIONS **734** CITATIONS
SEE PROFILE

Giuseppe Pappalardo
Italian National Research Council
84 PUBLICATIONS **1,480** CITATIONS
SEE PROFILE

European Journal of Medicinal Chemistry 81 (2014) 442–455

Contents lists available at ScienceDirect

European Journal of Medicinal Chemistry

journal homepage: http://www.elsevier.com/locate/ejmech

Original article

Molecular and cytotoxic properties of hIAPP17–29 and rIAPP17–29 fragments: A comparative study with the respective full-length parent polypeptides

Marianna Flora Tomasello [a], Alessandro Sinopoli [b], Francesco Attanasio [a], Maria Laura Giuffrida [a], Tiziana Campagna [a], Danilo Milardi [a], Giuseppe Pappalardo [a,*]

[a] CNR-Institute of Biostructures and Bioimaging, Via P. Gaifami 18, 95126 Catania, Italy
[b] International PhD Program in Translational Biomedicine, University of Catania, V.le A. Doria 6, 95125 Catania, Italy

ARTICLE INFO

Article history:
Received 14 November 2013
Received in revised form
11 April 2014
Accepted 11 May 2014
Available online 14 May 2014

Keywords:
Spectroscopy
Type 2 diabetes
Confocal microscopy
Mitochondria
Amyloid
Model membranes

ABSTRACT

The human islet polypeptide (hIAPP) or amylin is a 37-residue peptide hormone secreted by β-cells of the islet of Langerhans in the pancreas. Unlike the rat variant of IAPP (rIAPP), human amylin is highly amyloidogenic and is found as amyloid deposits in nearly 95% of patients afflicted with type 2 diabetes mellitus (T2DM). Human and rat IAPP have nearly identical primary sequence differing at only six positions which are encompassed within the 17–29 aminoacid region. Using Circular Dichroism (CD), Dynamic Light Scattering (DLS) and ThT-fluorescence (Th-T), we examined the aggregation properties of both full-length hIAPP1–37 and the related peptide fragment hIAPP17–29. For the sake of comparison, similar experiments were carried out on the respective rat variants rIAPP1–37 and rIAPP17–29. These studies were conducted at physiological pH in buffered solution not containing fluorinated co-solvents as well as in the presence of model membranes (LUV). In addition, the cytotoxic activity of the investigated peptides was determined toward different pancreatic β-cell lines. All the peptide studied in this work resulted cytotoxic despite β-sheet structure being observed, in vitro, for the hIAPP1–37 only. This suggests that β-sheet conformational transition that generally precedes the fibril formation, is not a prerequisite for toxicity towards β-cells. Interestingly, confocal microscopy indicated that the IAPP peptides can enter the cell and might exert their toxic action at an intracellular level.

1. Introduction

Among proteins conformational diseases, Alzheimer's and Parkinson's diseases, prion diseases, Amyotrophic lateral sclerosis (ALS), and several other less known pathological conditions, share the abnormal deposition of fibrillar protein aggregates within tissues [1,2]. A clinical hallmark in more than 95% of patients suffering from type II diabetes mellitus (T2DM) is the accumulation of fibrillar material in the pancreatic islet of Langerhans [3]. Due to this clinical feature, T2DM has been also included among the amyloid diseases [4]. The main component of the pancreatic amyloid deposits is a 37-residue polypeptide hormone called Islet Amyloid Polypeptide (IAPP) or amylin [5]. In humans, IAPP is synthesized as a 67-residue pro-peptide and co-localize with insulin in the secretory granules of pancreatic β-cells of the islets of Langerhans. The soluble form of mature (37-residue polypeptide) IAPP is believed to play a role as regulator of glucose homeostasis and has been found to be released following an increase in blood glucose level [6]. Human IAPP (hIAPP) possesses a particularly high propensity to misfold into cytotoxic aggregates that evolve into mature fibrils, with time. The growth mechanism of fibrils is well recognized through a multistep seed/nucleation process that involves key soluble oligomeric intermediates and protofibril states [7–9]. It is widely accepted that all toxicity is caused by small soluble oligomers that precede the growth of β-conformation rich mature fibres [10–12]. Mature fibrils tend to accumulate outside the cell

Abbreviations: hIAPP, human islet amyloid polypeptide; IAPP, islet amyloid polypeptide; MTT, 3-(4,5-dimethylthiazol-2-yl)-2,5-diphenyltetrazolium bromide; rIAPP, rodent islet amyloid polypeptide; DMSO, dimethylsulfoxide; Fmoc, 9-fluorenylmethoxycarbonyl; HFIP, 1,1,1,3,3,3-hexafluoro-2-propanol; HPLC, high-performance liquid chromatography; TFA, trifluoroacetic acid; ThT, Thioflavin-T; T2DM, Type 2 diabetes; LUV, large unilamellar vesicles; CD, circular dichroism; ESI-MS, electrospray ionization mass spectrometry; TMRM, Tetramethyl rhodamine methyl ester; *DCFH-DA* 2′,7′, dichlorfluorescein-diacetate; ROS, Reactive oxygen species; NAC, N-acetyl-L-cysteine.

* Corresponding author.
E-mail addresses: giuseppe.pappalardo@cnr.it, pappalardo.cnr@unict.it (G. Pappalardo).

http://dx.doi.org/10.1016/j.ejmech.2014.05.038
0223-5234/

where they are relatively inert, whereas toxic oligomers have been reported to form also intracellularly [13]. The way by which hIAPP exerts its cytotoxic action is not fully understood yet, membrane mediated hIAPP aggregation suggests that the formation of potentially toxic hIAPP species may be promoted in the presence of cellular membranes [14a]. Cellular membrane disruption is thought to occur through a variety of different mechanisms, including toroidal (doughnut-like) pore formation, induction of excessive negative curvature strain as well as detergent-like and carpet mechanisms [14b]. Growing support for involvement of oxidative stress in islet dysfunction and death has also been reported [15–17].

Interestingly, either antioxidant treatments or inhibition of fibril formation were effective in reducing ROS levels and β-cells apoptosis, suggesting that both molecular mechanisms might be involved in IAPP toxicity [16]. The importance of specific regions of the hIAPP for the self assembly, fibril formation and related cytotoxic action, has been extensively explored [8,18–20]. According to these studies, peptide regions corresponding to residues 8–20, 10–19, 17–29, 20–29 and 30–33 of human IAPP, have been identified as critical sites for amyloid growth [21–24]. Our previous work focused on the comparison of the conformational properties and aggregation behaviour of peptide fragments corresponding to the 17–29 aminoacid region of either human or rat IAPP (hIAPP17–29; rIAPP17–29) [25,26]. The choice of this peptide region was dictated by the fact that IAPP from rodents differs from the human polypeptide at six positions, all occurring between residues 17 and 29. The presence of three proline residues, in the rat variant, prevents the adoption of a β-sheet conformation required for fibril formation. Therefore, the full-length rIAPP is reported to be a monomer without a stable well defined structure in aqueous solution, not prone to self-aggregation and then not toxic to β-cells [27]. The kinetic of IAPP amyloid formation is not fully defined yet, and reasons for the conflicting results reported in the literature may depend on the wide range of sample preparation methods, some of which employed fluorinated alcohols as co-solvents [28]. Based on a sample preparation protocol that excludes the presence of fluorinated solvents, we have examined in this work the conformational features and aggregation properties of both full-length hIAPP1–37 and the related fragment hIAPP17–29 and compared the results with the respective rat counterparts. These studies were carried out by means of Circular Dichroism (CD) spectroscopy, Dynamic Light Scattering (DLS) and Thioflavin-T (Th-T) fluorescence. In addition, the cytotoxic activity of the studied peptides was determined towards pancreatic β-cells lines. On the whole, our results suggest that β-sheet conformational transition, which generally preludes the fibril formation, is not a prerequisite for toxicity towards pancreatic β-cells. Moreover, confocal microscopy reveals that exogenous IAPP peptides can enter the cell thus supporting the hypothesis that these peptides might exert their toxic action at an intracellular level.

2. Results

2.1. CD investigation of the IAPP peptides

Time course far-UV CD spectroscopy was used to monitor the conformational changes of the studied peptides in the event of fibril formation. All the peptide samples were subjected to a disaggregating procedure, described in the experimental, before starting any spectroscopic measurement. In Fig. 1A the CD curve profiles of hIAPP1–37 recorded at different interval times are reported. Consistent with literature data, freshly prepared samples exhibited at the beginning of incubation a CD spectrum characteristic of largely unstructured polypeptide chain. No significant changes were detected during the first 24 h. Conversely, the CD

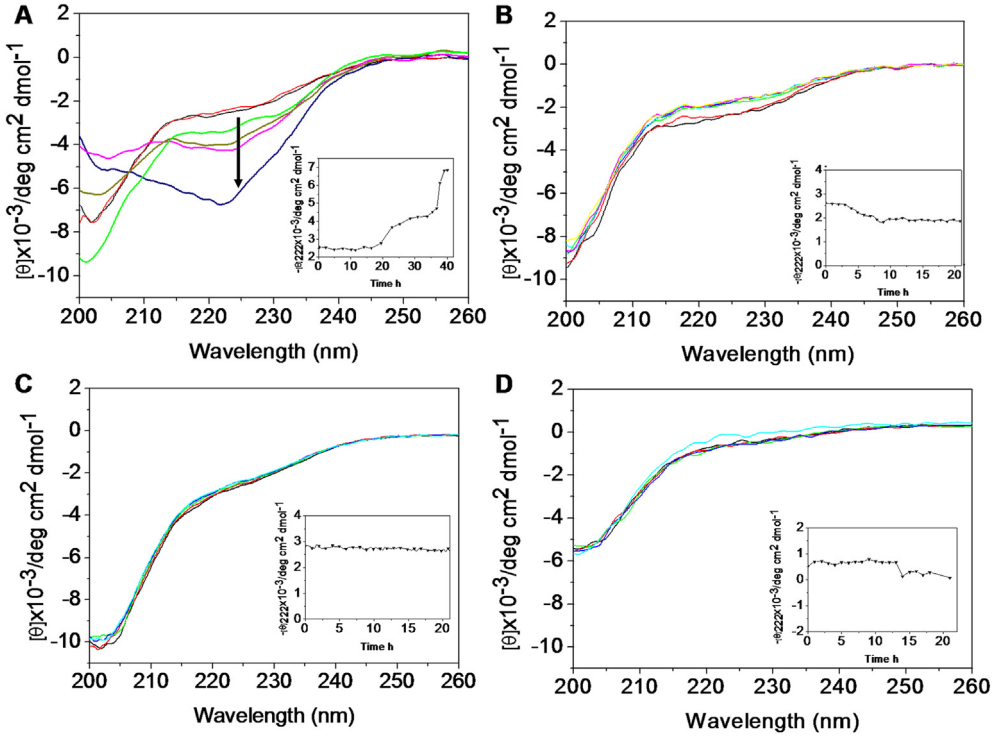

Fig. 1. A) CD spectra of hIAPP1–37 recorded at different time intervals (from 0 to 40 h). B) CD spectra of hIAPP17–29. C) CD spectra of rIAPP1–37. D) CD spectra of rIAPP17–29 recorded at different time intervals (from 0 to 21 h). The concentration of peptides was 20 μM in 2 mM phosphate buffer pH 7.0 at $T = 37$ °C. Insets represent the mean residue ellipticity at 222 nm as a function of time.

spectrum recorded after 40 h showed an intense negative signal at 220 nm indicating the transition towards β-sheet structures [29].

Concerning the hIAPP17–29 and the rat variants, our observations indicated the persistence of strong negative ellipticity around 200 nm and no significant modification of the initial CD profile were observed (Fig. 1B, C, D). Such a result, which is in agreement with the accepted notion that full-length rIAPP1–37 and rIAPP17–29 are not prone to aggregation, also indicates that in our experimental conditions the hIAPP17–29 exhibits a definitely reduced propensity to self-assembly.

An identical set of CD experiments were carried out in the presence of large unilamellar vesicles (LUV) made up with POPC (See Fig. S1). This was done to get an insight into the conformational changes that might occur in a membrane mimicking environment. The CD curve profile of freshly prepared 20 μM hIAPP1–37 in the presence of 200 μM of POPC was characterized by negative signals at 208 and 222 nm, which may indicate the presence of α-helical conformation [29]. However, the higher amplitude of the band at 208 compared to that one at 222 nm, together with the absence of positive ellipticity below 200 nm, strongly suggests the presence of significant amount of unstructured peptide chain. The hIAPP1–37 CD profiles reduced in intensity with time, without significantly varying the overall spectral pattern. The CD curve recorded after 24 h, displays almost comparable signals at 208 and 222 nm with no clear evidence of β-sheet conformational transition. A similar behaviour was observed in the case of hIAPP17–29: here the CD profiles were dominated by an intense negative signal around 202 nm that decreased with time. No signs of structured peptide conformation could be inferred from the CD data. Finally, the rat variants always displayed unchanged random coil CD spectra throughout the whole period of monitoring (Fig. S1).

2.2. Fibril formation measured by Thioflavin-T assay

Time dependent increase of Th-T fluorescence intensity of incubated IAPP peptides (20 μM) in the presence of 60 μM Th-T in 2 mM phosphate buffer pH 7.0, were carried out to investigate the kinetic of fibrillogenesis. In Fig. 2 the observed kinetic profile of hIAPP1–37 fits to a sigmoid curve. Here the presence of the lag-phase indicates the assembling and nucleation of monomers or small oligomers that generate protofibrillar forms during the exponential phase. On the contrary in the case of rIAPP1–37, as well as the shorter hIAPP17–29 and rIAPP17–29 peptides, the Th-T fluorescence intensity remains almost unchanged for the whole period of monitoring, thus indicating that no fibril formation occurs under these experimental conditions. An almost identical behaviour was observed in the presence of 200 μM POPC while the hIAPP1–37 was the only peptide able to form amyloid fibrils. Note that the presence of artificial POPC membranes markedly prolonged the lag phase duration of full-length hIAPP compared to the one observed in water solution (Fig. S2).

2.3. Dynamic Light Scattering (DLS)

The aggregation process of the IAPP peptides was further investigated by means of DLS. The hIAPP1–37 sample revealed the formation of aggregated species within a few minutes of preparing the solution. These aggregates show a hydrodynamic radius of about 90 nm. The absolute scattered intensity value (9.3×10^{-5} cm^{-1}) allows for an estimation of the initial aggregation number, which for hIAPP1–37 is around 1000. By comparing the measured hydrodynamic radius of the aggregate and that one estimated for the single hIAPP1–37 (about 2.5 nm), it is possible to deduce that almost all the population of hIAPP1–37 initially exists as oligomers and that the obtained aggregation number is consistent with a non-compact and fully hydrated structure [30]. During the 24 h of the experiment, the hydrodynamic radius increased up to micrometric dimensions as shown in Fig. 3. Interestingly, the rIAPP1–37 also showed aggregated forms with a hydrodynamic radius of about 130 nm. However, their size did not exceed the hydrodynamic radius of about 350 nm in the same time interval of 24 h (Fig. 3). The number of molecules, composing the initial rIAPP1–37 aggregates, is in the same range as hIAPP1–37. Size distribution of the aggregates for both hIAPP1–37 and rIAPP1–37 is reported at two different time intervals (2 and 300 min) in the Supplementary materials (Figs. S1A, B). A totally different behaviour with the fragments hIAPP17–29 and rIAPP17–29 was observed: no evidence of aggregated forms were found at anytime (data not shown). DLS measurements, carried out in the presence of 200 μM POPC were not informative because of the presence of an interfering high intensity scattering signal that may be assigned to LUVs. This signal was centred at around 150 nm (data not shown).

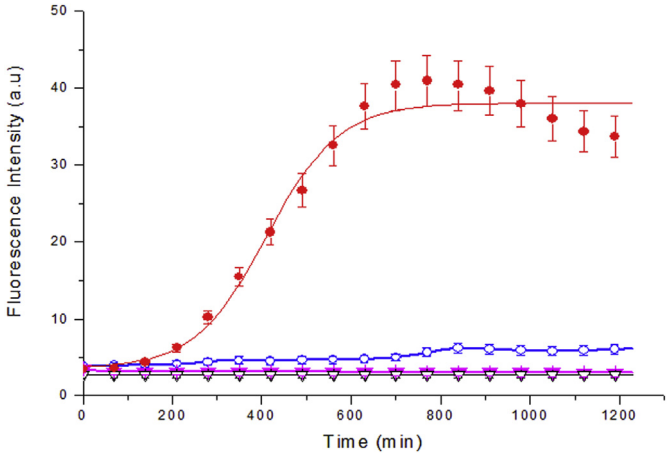

Fig. 2. Fibrils formation kinetics of hIAPP1–37 (filled circle), hIAPP17–29 (open circle), rIAPP1–37 (filled triangle) and rIAPP17–29 (open triangle) monitored by Th-T fluorescence. The concentration of the peptides was 20 μM in 2 mM phosphate buffer pH 7.0 at $T = 37$ °C.

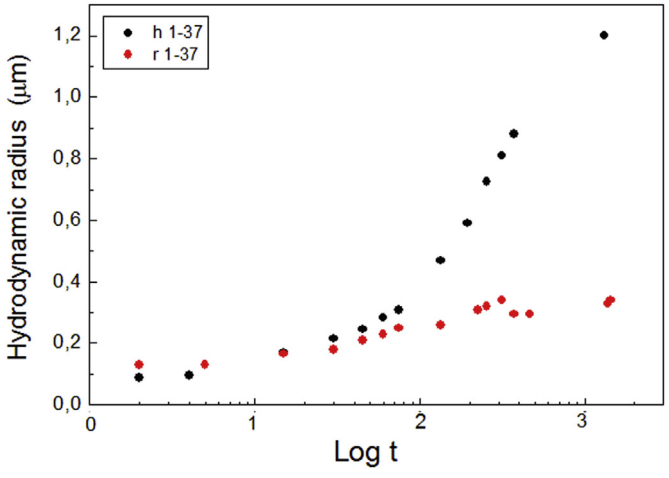

Fig. 3. The dependence of the hydrodynamic radius of hIAPP1–37 (filled circles) and rIAPP1–37 (filled triangles) aggregates on time. Peptides concentration was 20 μM in 2 mM phosphate buffer pH 7.0 at $T = 37$ °C. Time intervals logarithm of the time in minutes.

2.4. Cytotoxic potential of amylin peptides

Rat insulinoma cells lines (RIN-M and INS1) were exposed to either rat or human full length IAPP as well as to the respective 17–29 fragments. Cells were incubated for 48–62 h in the presence of increasing concentrations (0.1–100 μM) of each peptide, then the mitochondrial reductase activity was measured by using the MTT assay. Fig. 4A shows the dose-dependent response, measured for each peptide after 62 h of exposure. When treated with 1 μM hIAPP1–37, the MTT response of RIN-M cells was around 80% with respect to controls and decreased to 20% when 100 μM hIAPP1–37 was used. The hIAPP17–29 peptide also exhibited a dose dependent cytotoxic effect (with 80% at 12 μM and 60% at 100 μM) (Fig. 4A). Surprisingly, the non amyloidogenic rIAPP1–37 and rIAPP17–29 peptides were found to be cytotoxic to β-cells after 62 h of incubation. Charts in Fig. 4A, show that the dose response curves of human and rat IAPP1–37 are almost overlapping. In the same way the dose response trend exhibited by the rIAPP17–29 fragment is similar to the one of hIAPP17–29. Conversely, a scrambled peptide corresponding to the sequence of the rIAPP17–29 did not induce any toxic effect (Fig. S9). Experiments carried out using INS-1 cells gave analogous results (see Supplementary material Fig. S4).

It should be mentioned that in the case of shorter incubation times (24–30 h) significant cytotoxic responses were observed for the full-length human and rat IAPP1–37 only (not shown).

Since MTT reduction assay may reflect both reversible and irreversible cellular dysfunction, not always resulting in cell death, the toxicity of our peptides was also evaluated by using other methods. Mitochondrial membrane potential ($\Delta\Psi_m$) is a key indicator of cellular viability, as it reflects the pumping of hydrogen ions across the inner membrane during the process of electron transport. By using the nerstian dye TMRM, we found that treatment with hIAPP17–29 or rIAPP17–29, also induced $\Delta\Psi_m$ collapse (Figs. 5A and S6A). Determination of cellular ATP, considered as a hallmark of cell viability, proliferation, cytotoxicity and cell death, also revealed a dose dependent reduction in total ATP levels in RIN-M cells exposed to either hIAPP1–37 or rIAPP1–37. Again, analogous results were obtained when the respective 17–29 fragments were used (Fig. S5). PI staining measurements by flow cytometry (Figs. 5B and 6B) and morphological analysis by light microscopy (Fig. 5C) were also used to quantify the extent of membrane damage evoked by IAPP peptides. Fig. 5C shows the dramatic morphological alterations induced in RIN-M cells by either hIAPP1–37 or rIAPP1–37. Damaged cells were also detectable upon exposure to the hIAPP17–29 and the rIAPP17–29 fragments, even though some cells were still adherents. Nevertheless, flow cytometry revealed that, in almost 50% of cells exposed to 50 μM of either hIAPP17–29 or rIAPP17–29, the plasma membranes was disrupted, as cells stained positively to PI (Figs. 5B and 6B). Altogether, our data suggest that peptides corresponding to the 17–29 aminoacid sequence of both hIAPP and rIAPP were able to induce cell dysfunctions involving the impairment of the mitochondrial activity, as found for the respective full-length 1–37 parent peptides.

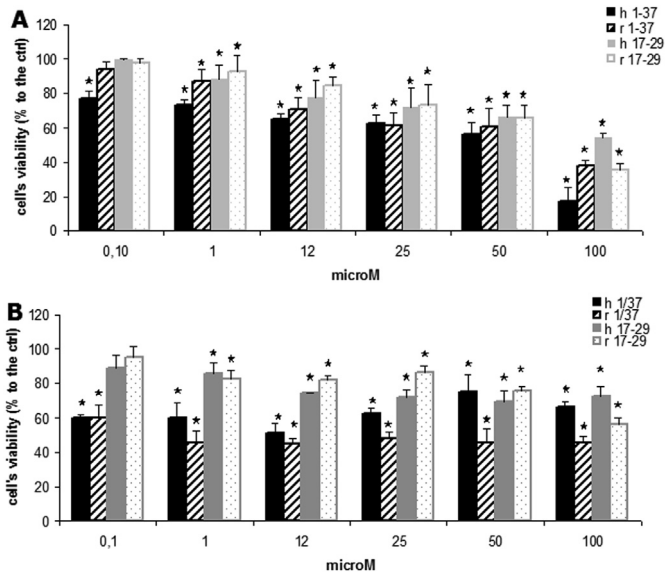

Fig. 4. Dose-dependent loss of mitochondrial (MTT) activity in RIN-M cells treated with 0.1–100 μM of freshly prepared (A) or aged (B) rIAPP1–37, hIAPP1–37, rIAPP17–29 and hIAPP17–29. Change in reductase activity is expressed as percentage to the control made using peptide-free vehicle (DMSO). Each value represents mean ± SD of five independent experiments. Significant difference from control value was indicated by $^*(p < 0.05)$ (one-way ANOVA with Tukey's post hoc test).

2.5. IAPP's toxicity toward β-cell and in vitro peptide conformation

The ability of hIAPP to self-assemble into cytotoxic molecular species is considered a central event contributing to β-cells loss in type 2 diabetes [31,32]. As we measured a cytotoxic response by also treating cells with the non aggregating rat peptides, we wondered how pre-incubating either hIAPP1–37 and 17–29 or the rat variants would affect the viability of cultured RIN-M cells. Based on the CD results, β-sheet conformation was only observed for the hIAPP1–37, in the absence of membrane and after 40 h incubation at 37 °C. It has been reported that incubation of amylin for 72 h, also referred to as "aged amylin", increased the amount of aggregated fibrillar forms [32]. Therefore we treated RIN-M cells with peptide samples that were pre-incubated in RPMI culture medium at 37 °C for 70 h. MTT was then measured in RIN-M cells after 62 h of incubation in presence of the "aged" amylin peptides. Also in this case we found reduced mitochondrial reductase activity in RIN-M cells, but the dose dependent response was lost (Fig. 4B). Again, the cytotoxic effect of the non-β-sheet-forming rat sequences rIAPP1–37 and rIAPP17–29 was comparable to that of the corresponding human sequences. This suggests that cytotoxic effects are not strictly related with the IAPP peptides' ability to form β-sheet aggregates in vitro. Such a result is comparable to what was recently reported by Magzoub and Miranker who showed that rIAPP, like hIAPP, is cytotoxic [33].

2.6. IAPP-induced production of ROS

The signalling pathway implicated in islet dysfunction and cell death is generally believed to include phenomena such as the overproduction of reactive oxygen species (ROS) [34]. To investigate whether reduction of the ROS levels might prevent IAPP-induced cell death, we cultured RIN-M cells in the presence of N-acetyl-L-cysteine (NAC). NAC was used at the highest possible concentration not affecting cell viability (10 mM) and cell was exposed to NAC 15 h before treatments with the IAPP peptides. The effect of NAC pre-treatment on IAPP-mediated cytotoxicity was then determined following 62 h exposure of the cells to the toxic peptides. We found that NAC almost completely blocked the progression of IAPP-induced cell death (Fig. 6A).

To validate the hypothesis that exposure of β-cells to the IAPP peptides may result in increased ROS levels, we cultured RIN-M in the presence of the hIAPP17–29 and rIAPP17–29 peptides and then measured ROS levels by using the ROS probe DCFH (see the experimental procedures section). We found that intracellular ROS levels increased and reached a maximum value within 60 min from the initial treatment. After 60 min, ROS returned to the basal level

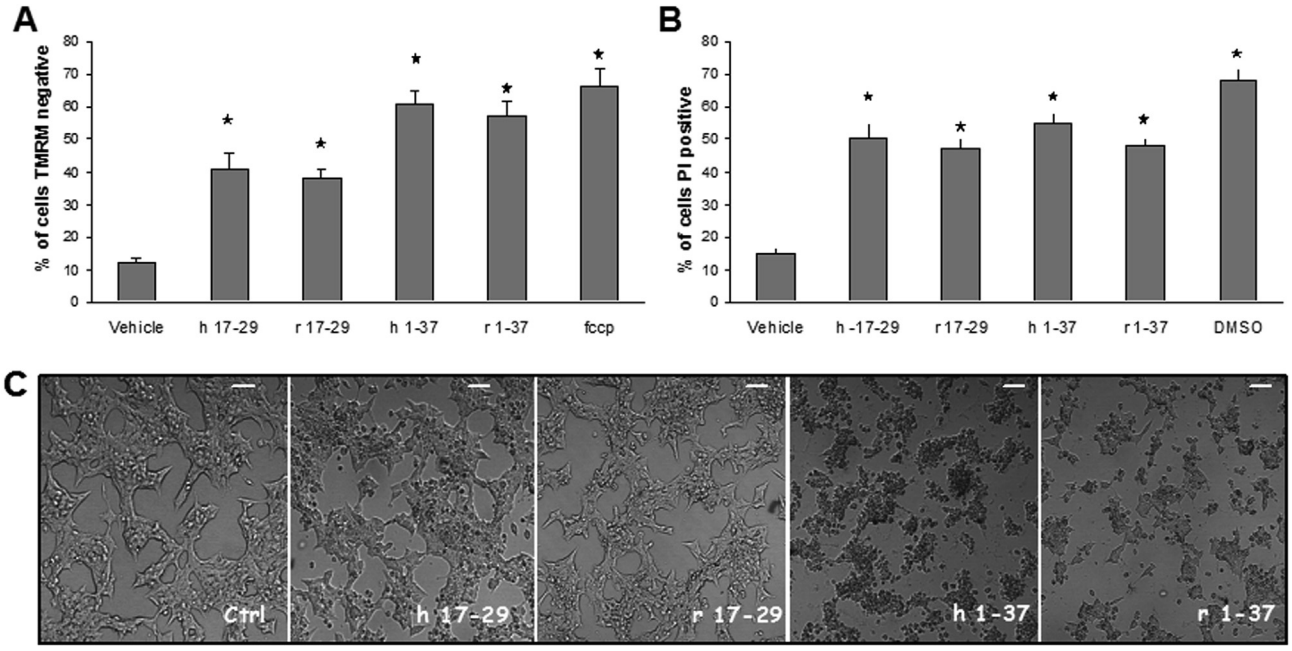

Fig. 5. *A*) Effect of IAPP peptides on mitochondrial $\Delta\Psi_m$. RIN-M cells treated for 62 h with 50 μM of freshly prepared hIAPP17–29 or rIAPP17–29 and incubated with TMRM to monitor $\Delta\Psi_m$ by flow cytometry. 1 μM FCCP (15 min) was used as a depolarizing control. *B*) Effect of IAPP peptides on plasma membrane integrity monitored as permeability of cells to PI. RIN-M cells treated for 62 h with 50 μM of freshly prepared hIAPP17–29, rIAPP17–29, hIAPP1–37 or rIAPP1–37, incubated with PI and examined in FL3 mode by flow cytometry. 10% DMSO was the positive control. At least 20,000 events were scored for each group. Experiments were done in triplicate. *Bars: S.E.M*, * indicates a significant difference ($p < 0.001$, χ^2 *test*). C) Phase contrast images of RIN-M cells treated for 62 h with 50 μM of freshly prepared amylin peptides: rIAPP17–29, hIAPP17–29, rIAPP1–37 and hIAPP1–37. Both rIAPP1–37 and hIAPP1–37 induced dramatic aberrations in cell morphology reproduced to a lesser extent also by rIAPP17–29 and hIAPP17–29. Scale bar, 10 μm.

(not shown), probably due to the activation of the intracellular antioxidant system (Fig. 6B). Our data are in keeping with the hypothesis that IAPP may exert its pro-apoptotic effects by generating ROS [35].

2.7. Subcellular localization of IAPP peptides

The question as to whether IAPP peptides act intra or extracellularly is still debated. By using two complementary approaches, i.e. the use of fluorescent labelled peptides and the immunocytochemistry, we attempted to visualize the sub-cellular distribution of the IAPP peptides in RIN-M cells. Concerning the use of fluorescent peptides we obtained an F-hIAPP1–37 sample from a commercial source (Anaspec), while the F-hIAPP17–29 and F-rIAPP17–29 were synthesized by us. The F-hIAPP17–29 and F-rIAPP17–29 were purified and characterized by means of CD and ESI-MS techniques, before carrying out any biological experiment (see Supplementary material Fig. S7). The F-hIAPP17–29 and the F-rIAPP17–29 cytotoxic activity reproduced what measured for the corresponding unlabelled peptides (Fig. S8).

RIN-M cells were imaged by confocal microscopy after 20–60 min incubation at 37 °C in the presence of 25 μM of the F-hIAPP1–37 or F-hIAPP17–29 or F-rIAPP17–29. In these conditions distinct fluorescent puncta (Figs. 7A and S11A) at the cell surface, reminiscent of membrane-bound peptide, were seen in all cases studied. Weak fluorescent spots were also detectable inside cells where the fluorescent peptides were excluded from the nucleus. Such a distribution pattern may suggest that the molecular species at the cells surface represent an early step preceding the intracellular uptake. A similar uptake was observed when the incubation was carried out at 4 °C where endocytosis and other energy-dependent uptake processes are inhibited, thus suggesting an energy-independent, uptake mechanism (not shown). Changes in the cell morphology, characterized by the appearances of elongated protrusions, were frequently observed and the binding/uptake of fluorescent IAPP was especially noticeable in these protrusions (Fig. 7A). This may suggest that both F-hIAPP1–37 and F-hIAPP17–29 accumulate at specific microdomains on the cell plasma membrane, where the peptide uptake follows. These microdomains have often been suggested to correspond to lipid rafts [36]. Interestingly, changes in cellular distribution were observed after 1 h incubation for all the fluorescent peptides and the localization pattern indicated a perinuclear distribution (suggestive of either mitochondria or lysosomes). Both mitochondrial and lysosomal targeting of IAPP peptides have been reported [33]. Interestingly we found that both F-hIAPP17–29 and F-hIAPP1–37 colocalized with mitochondria (Fig. 7B and C), whereas the labelled F-rIAPP17–29 targeted lysosomes (Fig. S11B and C).

However, few minutes after the F-hIAPP1–37 or the F-hIAPP17–29 localized at mitochondria, the MitoTracker staining diffused throughout the cytosol. This phenomenon was quickly followed by the leakage of either F-hIAPP1–37 or F-hIAPP17–29 from mitochondria. At 120 min both signals (the MitoTracker probe and the fluorescent IAPP peptides) spread throughout the cytoplasm indicating that mitochondria were impaired (Fig. 8A and C). Finally, signals vanished after 200 min (Fig. 8A).

Spread cytosolic fluorescence was also observed following 120 min incubation with the labelled F-rIAPP17–29 (Fig. S11C). This was also accompanied by nuclear condensation (DAPI – Fig. S11C), changes in cell morphology and cell death. Under our condition we never observed co-localization between the human peptides and lysosome as well as the rat peptides and the mitochondrial compartment.

The incubation of either the labelled peptides for more than 3–4 h always produced the diffuse cytosolic staining shown in Fig. 8D or Fig. S11C. Morphological changes associated with apoptosis (blebs) just appeared during these prolonged incubation times (Fig. 8D and S11C) and some cells with cytosolic F-hIAPP1–37 or F-

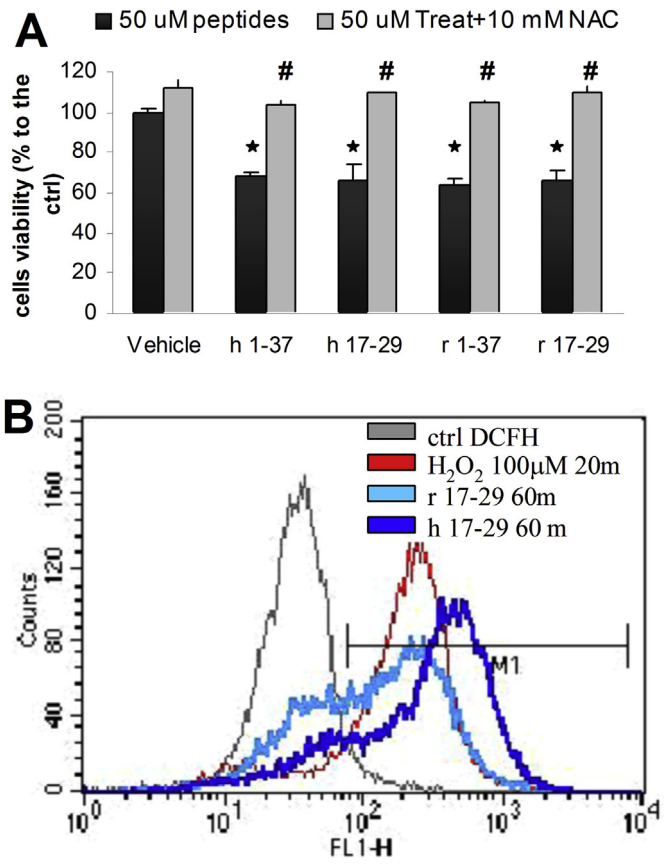

Fig. 6. *A)* NAC abrogates the IAPP-induced cell death. Cell viability (MTT) of RIN cells treated for 62 h with 50 μM hIAPP1–37, hIAPP17–29, rIAPP1–37 and rIAPP17–29 alone (black columns) or following pre-treatment (15 h) period with the antioxidant NAC (grey columns). Each value represents mean ± SD of five independent experiments. Significant difference from the control value was indicated by $^{*}(p < 0.05)$ (one-way ANOVA with Tukey's post hoc test). #, indicates significative difference ($p < 0.05$) (one-way ANOVA with Tukey's post hoc test), between sample with or without NAC. *B)* IAPP induced ROS generation as indicated by increase in DCFH fluorescence monitored by flow cytometry. RIN-M cells incubated for 1 h with 50 μM of freshly prepared hIAPP17–29 or rIAPP17–29 were loaded with DCFH and monitored by flow cytometry on FL1. 100 μM H_2O_2 (20 min) was used as a positive control. Curves represent the average fluorescence intensity profile for each population. At least 20,000 events were scored for each group. Experiments were done in triplicate.

hIAPP17–29 turned permeable to the PI dye which can only enter dying cells (Fig. 8E).

The subcellular distribution of the exogenously added IAPP or endogenous IAPP was also explored in RIN-M cells by immunocytochemistry and confocal microscopy using a specific IAPP antibody. The potential formation of intracellular IAPP oligomers was detected by using the oligomers-specific A11 antibody. This antibody reacts with soluble proteins or peptide oligomers, but does not react with monomers or fibrils [37]. Immunofluorescence analysis revealed that staining of endogenous IAPP was stronger near the plasma membrane especially in protrusion and extensions of non-treated RIN-M cells (Fig. 9A). When cells were incubated with 25 μM of synthetic IAPP17–29 peptides for 3–4 h, the immunostaining revealed a more intense intracellular (cytosolic) signal with an evident nuclear exclusion (Fig. 9A and B show the case of hIAPP17–29 peptide). Interestingly, oligomers were uniquely detected inside RIN-M cells treated with either hIAPP17–29 or hIAPP1–37 and exhibited a perinuclear distribution somewhat recalling mitochondria (Fig. 9C). The mitochondrial distribution of hIAPP1–37 oligomers was confirmed by colocalization with the MitoTracker probe. However, in some cases the MitoTracker was only slightly retained in mitochondria, most likely because of the mitochondrial impairment caused by hIAPP toxicity (Fig. 9C). Non-treated RIN-M cells (or cells treated with the rIAPP17–29) did not react with the A11 antibody, proving that oligomers are only formed by the exogenous hIAPP17–29 (not shown). The omission of either the oligomer-specific primary antibody A11 or the primary antibody against IAPP, completely removed the staining, thus confirming the specificity of the results.

3. Discussion

The ability of hIAPP to self-assemble into cytotoxic molecular species is considered a central event contributing to pancreatic β-cells loss in type 2 diabetes [38]. The analysis of hIAPP and rIAPP primary sequence indicates that the region corresponding to residues 18–29 is a key determinant for hIAPP to form amyloid [38]. Notably, rIAPP contains in this region three proline residues that prevent the adoption of a β-sheet structure by the peptide chain; thus IAPP from rodents is soluble in aqueous environment, does not readily aggregate and consequently is generally used as a non-cytotoxic control. In this work we have comparatively studied the conformational and cytotoxic properties of the two hIAPP17–29 and rIAPP17–29 peptides with reference to their respective full-length 37-mer parent peptides. The kinetic of hIAPP amyloid formation is very sensitive to experimental conditions and sample preparation. Our previous studies highlighted the ability of hIAPP17–29 to form amyloid species as a function of the pH. More specifically, the rate of assembly and morphology of the hIAPP aggregates was modulated by the ionization state of His-18, and this result was in agreement with Abedini and Raleigh observations [25,26,39]. However in these studies, in order to achieve a clear sample solution of the fibrillogenic peptide, fluorinated alcohols (TFE or HFIP) were used as co-solvents. It is now well established that even 1% by volume of these co-solvents has a significant effect in inducing amyloid peptides aggregation by decreasing the lag time period and enhancing electrostatic interactions [40]. The protocol used in the present work to prepare the peptide samples excludes the presence of fluorinated solvents in the final solution and this may account for the obtained different results. In our experimental conditions the CD and Th-T of both human and rat IAPP1–37 samples, exhibited initially random coil curve profiles and low fluorescence intensity, whereas the DLS measurements indicated the presence of small aggregated species in the freshly prepared solution. The early formation of fully hydrated oligomeric species gives an explanation for these apparently contrasting results: in fact as reported in the literature oligomers may not be detected by the Th-T assay [41,42]. These aggregated forms appear also loosely packed with an high degree of hydration so that the peptide chains can freely adopt random conformations. Conformational β-sheet transition and enhancement of the Th-T fluorescence intensity matched the increasing size of the hIAPP1–37 aggregates, thus suggesting fibril formation for this peptide. It is interesting to note that although rIAPP1–37 can form aggregated species of comparable size to those of hIAPP1–37, rIAPP1–37 aggregates did not evolve into larger species or fibrils. This might be of relevance in view of the observed cytotoxicity of rIAPP1–37. Unlike the full-length peptides, the DLS analysis of the shorter hIAPP17–29 and rIAPP17–29 fragments proved that these peptides, during the monitoring period, did not form aggregated species. This was in keeping with the CD and Th-T results obtained for these peptides. For a more realistic picture of what might happen at the cell membrane interface with our IAPP peptides, we run the CD and Th-T kinetics also in the presence of model membranes. It turned out that in the presence of LUV made up with POPC, hIAPP1–37 was the only peptide able to form amyloid aggregates, in that reproducing

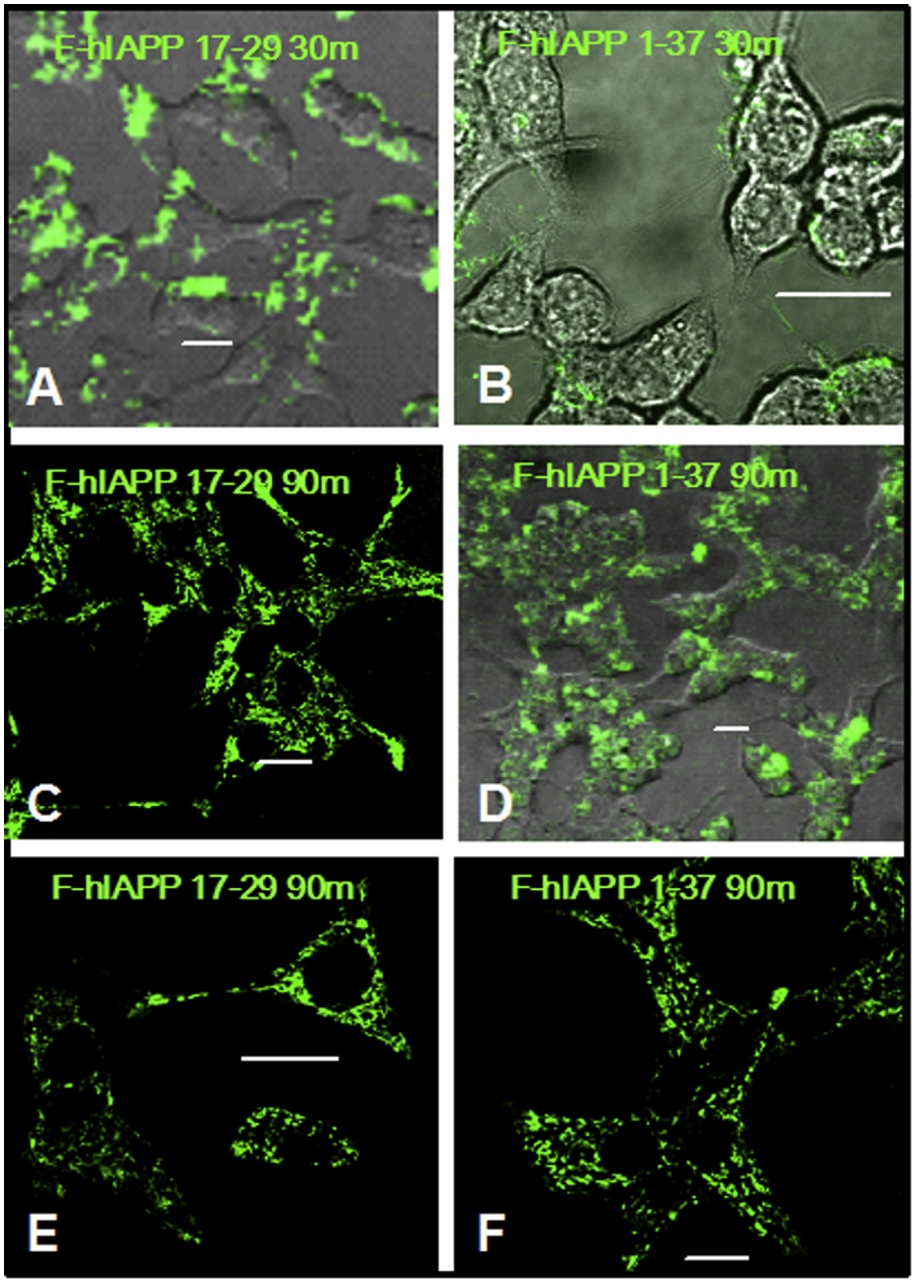

Fig. 7. Confocal microscopy analysis of hIAPP internalization and accumulation in cultured RIN-M cells. *A and B)* RIN-M imaged after 30 min of incubation with 25 μM of F-hIAPP17–29 (*A*) or 25 μM of F-hIAPP1–37 (*B*). Fluorescence accumulation on the cell surface was detected in both cases. Note that IAPP staining is especially noticeable in protrusions *C and D*) Mitochondrial targeting of both F-hIAPP17–29 (*C*) and F-hIAPP1–37 (*D*) after 90 min of incubation. *E and F*) Magnification of images showing the mitochondrial targeting of F-hIAPP17–29 (*E*) or 25 μM F-hIAPP1–37 (*F*) after 90 min of incubation. Images are representative of 30 cells analyzed for each condition in experiments performed in triplicate. Scale bar, 10 μm.

the same behaviour observed in buffer solution. No clear sign of β-sheet structure was noticed in the CD curves of the IAPP peptides in agreement with our hypothesis that the formation of this structure is not a requirement for the observed cytotoxicity.

It should be said, however, that the lack of aggregation we observed for hIAPP17–29 under our experimental conditions, does not mean that this peptide fragment is not amyloidogenic. Our results indicate that the sample preparation protocol we adopted, allows us to obtain soluble peptide samples, in the range of μM concentrations, containing monomeric hIAPP17–29.

Recent studies on hIAPP have shown that, in the absence of organic solvents and with the exclusion of preformed seeds, the CD spectra of peptide samples solubilized in water remain stable for many days. The peptide exhibited a random coil structure suggesting an unfolded state in aqueous medium [43,44]. In line with these reports and with our CD and DLS data, we found that all the IAPP peptides studied here were found to be significantly cytotoxic to β-cell lines after 48 h. Again, the lack of a direct correlation between the physico-chemical properties and the cytotoxic activity measured for our peptides supports the assumption that β-sheet aggregates might not be responsible for cytotoxicity. In any case, we cannot determine the conformational state adopted by the IAPP peptides upon interaction with the cell cultures but we found positive response between the A11 anti-oligomer antibody and the

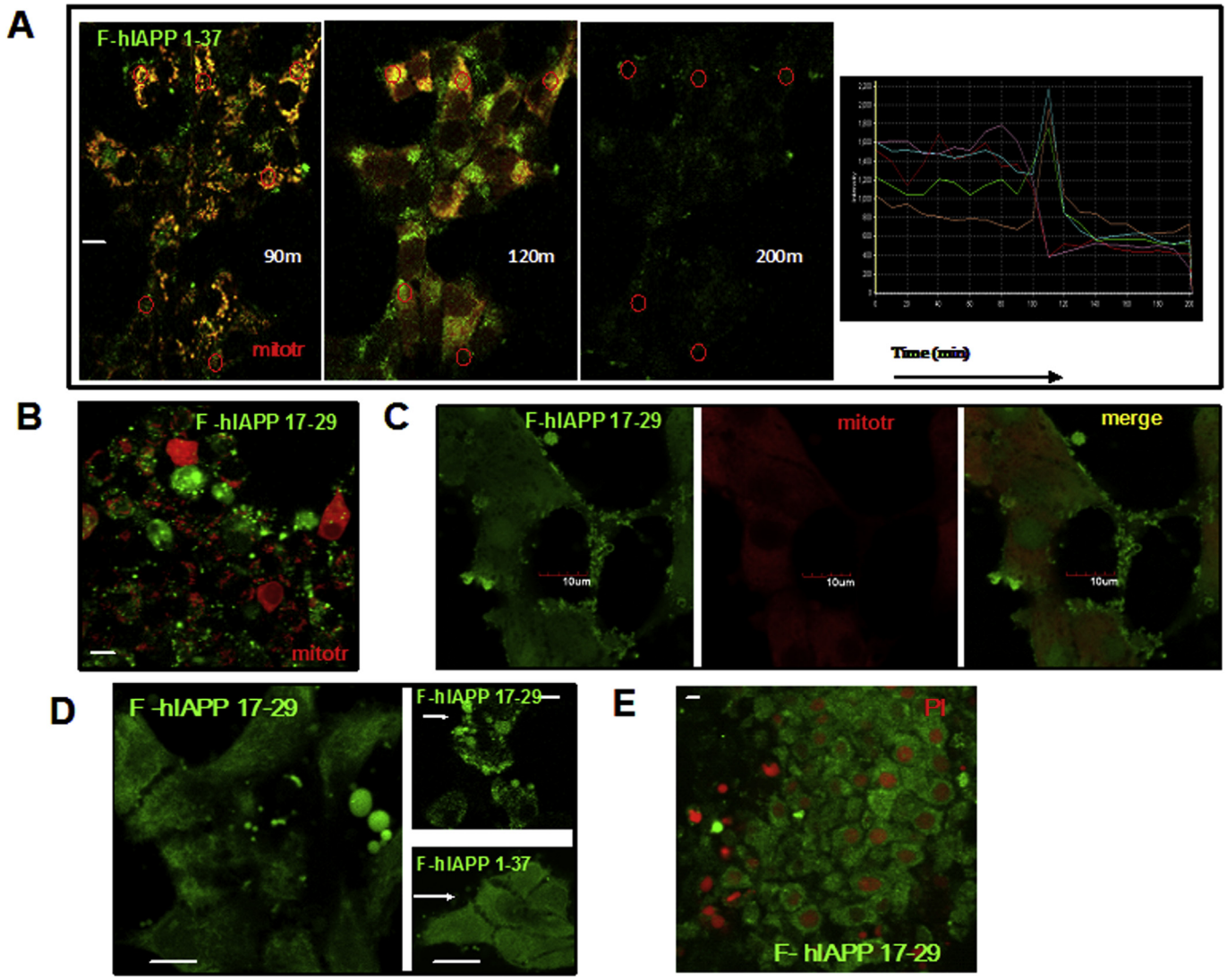

Fig. 8. Mitochondrial targeting of F-hIAPP1–37 *A)* and F-hIAPP17–29 *B*) was confirmed by coincubation with MitoTracker. In (*A*), representative images of a time lapse co-incubation with 25 μM F-hIAPP1–37 and MitoTracker are shown. Images, taken after 90 min and 100 min, indicate the co-localization of F-hIAPP1–37 (green) with MitoTracker (red). Incubation for 120 min resulted in the lost of MitoTracker staining and in the leakage of the F-hIAPP1–37 from mitochondria. Images were analyzed by drawing regions around individual cells and measuring the value of fluorescence as shown in the chart in the last panel. Values represent the average fluorescence measured inside the cell corrected from the basal fluorescence. Note that around 110–120 min the signal drops in some of the regions and boosts in some others. The drop reflects the decrease of the signal in regions corresponding to mitochondria, whereas the signal increases in regions corresponding to the cytoplasm. This is the result of the redistribution of F-hIAPP1–37 form mitochondria to the cytoplasm. After 200 min the signal drops in both mitochondrial and cytosolic regions. (*B and C*): The same result was obtained following the incubation of RIN-M with 25 μM F-hIAPP17–29. Note that IAPP staining is especially noticeable in protrusions. *C*) after 2 h of incubation, the F-hIAPP17–29 signal appears diffuse throughout the cytoplasm. (*D*) Note that 3–4 h of incubation with either F-hIAPP17–29 or F-hIAPP1–37 produced morphological changes associate with apoptosis. Blebs are evident especially in the magnified panels (arrows in the right panels). *E*) Cells with cytosolic F-hIAPP17–29 (green) and positive to the PI dye (red) which can only enter dying cells. Images are representative of 30 cells analyzed for each condition in experiments performed in triplicate. Scale bar, 10 μm. (For interpretation of the references to colour in this figure legend, the reader is referred to the web version of this article.)

hIAPP1–37 or hIAPP17–29 added to β-cells. This fact indicates that hIAPP1–37 or hIAPP17–29 can assemble into oligomeric forms in an intracellular environment.

Interesting similarities between the short fragments hIAPP17–29 and rIAPP17–29 and the respective full-length polypeptides were found in this work. In agreement with literature data reported for hIAPP1–37 [33,45,46], hIAPP17–29 exhibited a dose dependant cytotoxicity toward the rat insulinoma cell lines we used (RIN-M and INS-1). Moreover, we found that also the rIAPP variants exhibited a cytotoxic activity comparable to that measured for the hIAPP peptides. Actually, the experimental evidence that rIAPP1–37 is not harmless to β-cells was also reported by others [33,47,48] and considering the high sequence homology of hIAPP1–37 and rIAPP1–37, an rIAPP-associated cytotoxicity could be conceivable.

Conversely, in the case of the two IAPP17–29 fragments the sequence homology is relatively low because the rIAPP17–29 contains all the mutated residues, making the differences between the rat and human IAPP primary sequences. As both peptides were toxic (at the used concentration), we wondered if the aminoacid residues, shared by the human and rat sequences, were responsible for the observed cytotoxicity. The SSNN motif spans the 19–22 region of both the human and rat IAPP sequences. These aminoacids are predicted to be part of a short β-turn in the human sequence also appearing exposed at the aqueous interface in the model hIAPP fibril [49]. The SSNN peptide was synthesized,

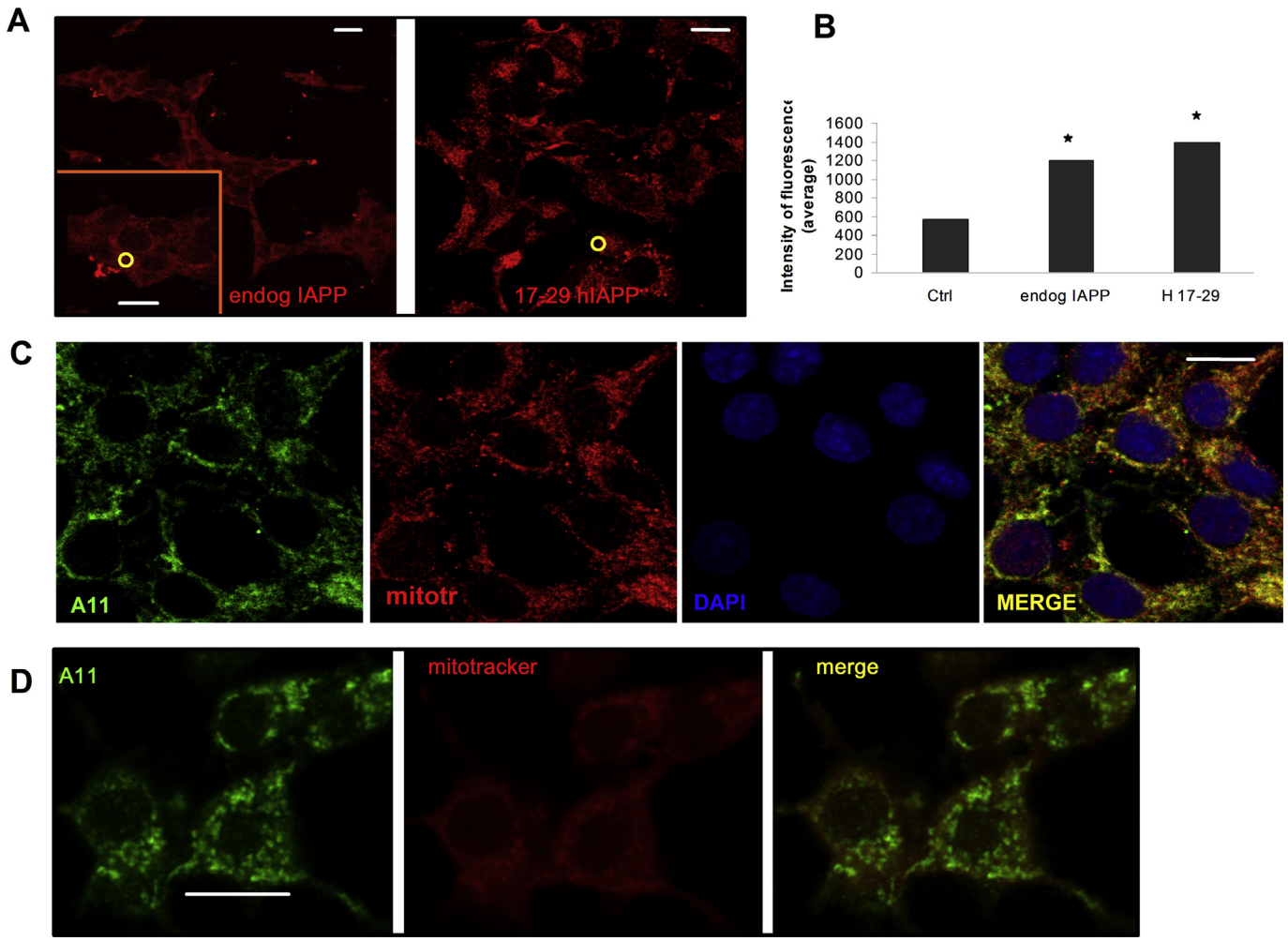

Fig. 9. *A)* RIN-M cells untreated (left panel) or exposed to 25 μM hIAPP17–29 (right panel), fixed and immunostained by using a specific antibody against IAPP (red). Images were analyzed by drawing regions around individual cells and measuring the value of fluorescence reported in *B*). Note the increased fluorescence intensity in cells exposed to 25 μM hIAPP17–29. The inset in the photograph in left panel is a magnification of the same image. *C*) Images represent three colours analysis of RIN-M cells exposed to 25 μM hIAPP1–37 and stained using the oligomers-specific A11 antibody (green), MitoTracker (red) and DAPI (blue). *D*) Two colours analysis of RIN_M cells treated with 25 μM hIAPP17–29 and stained using the A11 antibody (green) and MitoTracker (red). The co-localization appears weak in (*D*) as a consequence of the $\Delta\Psi_m$ collapse induced by IAPP exposure. Images are representative of 30 cells analyzed for each condition in experiments performed in triplicate. Scale bar, 10 μm. (For interpretation of the references to colour in this figure legend, the reader is referred to the web version of this article.)

purified and processed in the same way as the other peptides, to ensure that eventual aggregates were removed before application to cultured RIN-M cells. It turned out that viability of cells was not affected after 62 h of exposure to increasing concentration (12–100 μM) of SSNN (see Supplementary material Fig. S11). This suggests that this short motif cannot be, *per se*, the region responsible for the cytotoxic properties of IAPP. In addition, we did not observe toxic effects towards β-cells by a scrambled sequence of the rIAPP17–29 (Ac-SPLVPNGRLSPVN-NH_2, Fig. S12). The above results demonstrate that the rIAPP17–29 associated cytotoxicity is not just an artefact.

It should be pointed out that our findings do not exactly trace what was already reported by other authors [33], probably because the experimental conditions employed by us diverge in some crucial aspects. First, our peptide samples were subjected to an appropriated disaggregating procedure before carrying out each experiment. This procedure ensures the removal of any pre-existing aggregated form, and might be the reason why the hIAPP appears to be less toxic than the previous work. Secondly, the cell lines used in the present study are different.

A further aspect that should be taken into account is related to the peptide concentrations we used to measure the cytotoxic activity. β-cell administration of up to 100 μM exogenous IAPP may appear quite far from being physiologically relevant, even if mechanisms that protect against the strong amyloidogenicity of IAPP must exist in the secretory granule where IAPP is present at millimolar concentrations [50]. On the other hand the IAPP concentrations (i.e. 0.1–100 μM) we used in this work, were nearly in the same range of those reported by others. Indeed, cell viabilities values ranging from 15 to 80% can be found in the literature as the result of 5–25 μM, or even more, β-cells exposure to hIAPP1–37 for 24–48 h [9,45,48,51–53].

Neither the nature of the toxic species generated during IAPP amyloid formation, nor the mechanism of cell death are completely understood. Either receptor-mediated interactions or non-receptor mediated phenomena have been reported in the literature [54]. The elucidation of a detailed IAPP mechanism of toxicity is beyond the scope of this paper, but our evidence of small aggregated forms also in the rIAPP1–37 sample may be related with the observed cell toxicity for this peptide. Yet, recent papers dealing with full-length

rIAPP/membrane interaction may support this hypothesis because membrane disruption and permeabilization by soluble aggregated forms has been proposed to be linked to IAPP-mediated β-cell toxicity [14,31,55–57].

A toxic form of rIAPP1–37 has the potential to alter the interpretation of many results where this material is a negative non-toxic control. Very recent work attempted to establish the relationship between the observed cytotoxicity of rIAPP1–37 and rIAPP8–37 and their ability to form aggregated species [47]. Authors observed that, in analogy to hIAPP, rIAPP toxicity could be inhibited by an amylin receptor antagonist (AC 187) and a caspase inhibitor (zVAD-fmk). In addition they did not rule out any possible contribution of rIAPP oligomeric species to the toxicity of their preparations [47]. Our rIAPP preparations were always easily dissolved in water and the CD spectra did not change with time invariably showing an unstructured peptide conformation. In addition, our present and past work indicated that rIAPP17–29 did not interact with neutral or negatively charged artificial membranes [25]. This suggests once more that β-sheet formation is not a stringent prerequisite for the observed rIAPP17–29 cytotoxicity. The negative immunostaining with the A11 antibody in the β-cell treated with rIAPP17–29 is in keeping with the in vitro evidence that no aggregated forms could be detected by the CD and DLS experiments we carried out. At the moment the hypothesis that rIAPP17–29 toxicity might relate to a different mechanism, with respect to hIAPP, seems the more appropriate.

The confocal microscopy analysis carried out with the IAPP fluorescent peptides provided a number of interesting additional findings. First, all of our fluorescent IAPP peptides rapidly entered RIN-M cells. Secondly, images taken at different time intervals, revealed an initial accumulation of the fluorescents hIAPP1–37 and hIAPP17–29 peptides at the cell surface that may be interpreted in terms of IAPP peptide chains starting oligomerization at the membrane surface [58,59]. Then IAPP peptides were internalized and gained access to the mitochondrial compartment where they caused dysfonctions. F-hIAPP17–29 and F-hIAPP1–37 might penetrate the plasma membrane either by transduction or by endocytosis. The lack of a vesicular pattern on most of the confocal images after 30 min of incubation and the uptake of both the fluorescent peptides at 4 °C support the lack of an energy-dependent endocytosis mechanism. However, at the moment we cannot exclude other uptake dynamics.

Interesting observations were also made concerning the distribution of the fluorescently labelled rIAPP17–29. For short incubation times (30–90 min), the fluorescent peptide was detected either at the cellular surface, in this respect F-rIAPP17–29 behaves as the human counterparts, or within lysosomes. Lysosome localization represents an F-rIAPP17–29 peculiarity as we never observed in our conditions the human fluorescent IAPP peptides within these organelles. In agreement with our data, the fluorescent rat IAPP was detected by Magzoub and Miranker in the lysosomal/endosomal compartment whereas hIAPP was not [33]. As Magzoub and Miranker hypothesized, rat IAPP can be endocytosed and accumulated into lysosomes where it reaches a critical concentration, resulting in oligomerization, organelle membrane disruption and cytotoxicity. In line with this hypothesis we observed that prolonged incubation (2–3 h) of the F-rIAPP17–29 resulted in spreading of the fluorescent signal throughout the cytosol thereby suggesting the peptide has disrupted the lysosomal membrane. This event was associated with the condensation of nuclei and the appearance of other morphological alterations typical of apoptosis. We can conclusively speculate that both rat and human IAPP peptides might accumulate at the plasma membrane or in intracellular membranes such as mitochondrial or lysosomal membranes. In these sites, growing accumulation of peptides will result in the disruption of membranes, leakage of toxic molecules and cell death induction.

A recent hypothesis, to explain the ability of IAPP to enter the cell, invoked the formation of membrane bound α-helical aggregates endowed with cell penetrating features as a consequence of the clustering of positive charges from each IAPP peptide chain [45]. Our experimental evidence shows that also hIAPP17–29 enters the cell despite possessing only the histidine residue as possible cationising site. As expected for cationic molecules, both fluorescent F-hIAPP17–29 and F-hIAPP1–37 can be taken up into the mitochondrial matrix. The presence of this cationic peptide in the matrix leads to mitochondrial depolarization, opening of the permeability transition pore (PTP), swelling and rupture of the outer mitochondrial membrane, thus resulting in the rapid release of the peptide in the cytoplasm. In fact, mitochondrial swelling leads to the leakage of a serious of mitochondrial pro-apoptotic factors resulting in cell death [60]. These mitochondrial toxins selectively target the respiratory complexes I and II causing oxidative phosphorylation deficits and consequently an impairment of ATP production, oxidative stress, and energy deficits that ultimately cause cell death [61]. Disruption of the lysosomal compartment may also affect the redox balances of the cell. Oxidative stress has been involved in various neurodegenerative disorders associated with increased amyloidogenesis [62,63]. In agreement with this notion, in this work we have demonstrated that either the human IAPP peptides or the rat homologues caused ROS to increase. Moreover, cell death induced by IAPP is blocked by treatment with antioxidant compounds. Thus both the human and rat peptides appear as mitotoxic and cytotoxic molecules.

4. Experimental section

4.1. Materials

All N-Fmoc-protected aminoacids and TGR resin were purchased from NovaBiochem; 2-(1-H-benzotriazole-1-yl)-1,1,3,3-tetramethyluronium tetrafluoroborate (TBTU) and N-hydroxybenzotriazole (HOBT) were from Inbios; N,N-diisopropylethylamine (DIEA) and trifluoroacetic acid (TFA) were purchased from Fluka; piperidine, triisopropylsilane (TIS) and Th-T were purchased from Sigma/Aldrich; N,N-dimethylformamide (DMF) was purchased from Romil. All residues were introduced according to the HOBT/TBTU/DIEA activation method. A four-fold amino-acid excess was used for each coupling cycle. 1,2-Palmitoyl-oleoyl-sn-glycero-3-phosphocholine (POPC), was purchased from Avanti Polar Lipids with a purity of 99% and used without further purification.

4.2. Solid phase peptide synthesis

The peptides Ac-VHSSNNFGIALSS–NH_2 (hIAPP17–29) and Ac-VRSSNNLGPVLPP-NH_2 (rIAPP17–29), were synthesized on a CEM Microwave peptide synthesizer using a standard 9-fluorenylmethoxycarbonyl (Fmoc) chemistry as previously reported [25]. In the case of the synthesis of the F-hIAPP17–29 and F-rIAPP17–29 peptides the 5,6 Carboxyfluorescein (F) moiety was introduced at the N-terminus of the peptide chain by treating the fully assembled and protected peptide resin (after removal of the N-terminal Fmoc group) with a DMF solution (6 ml) containing a fourfold molar excess of 5,6 carboxyfluorescein, HOBT, TBTU and DIEA (69 μl). The fluorescent labelled peptides F-hIAPP17–29 and F-rIAPP17–29 were then deprotected and cleaved off from the respective solid support using a mixture of TFA/H_2O/TIS (95:2.5:2.5 v/v/v). Crude peptides were recovered by precipitation with freshly distilled diethyl ether. The purification of crude F-hIAPP17–29 and

F-rIAPP17–29 were carried out by Preparative reversed-phase high performance liquid chromatography (rp-HPLC) using a Varian Prepstar 200 Model SD-1 chromatography system equipped with a Prostar photodiode array detector with detection at 222 nm. A Vydac C_{18} 250 × 22 mm (300 Å pore size, 10–15 mm particle size) column was used. The peptides were eluted at a flow rate of 10 ml/min according to the following protocol: from 0 to 5 min isocratic conditions in 100% solvent A (H_2O containing 0.1% TFA) followed by a 15 min linear gradient from 0 to 40% B (CH_3CN containing 0.1% TFA) and then 5 min isocratic conditions in 40% B (rt F-hIAPP17–29 = 21 min; rt F-rIAPP17–29 = XXXX min). Fractions containing the desired product were collected and lyophilized. Analytical rp-HPLC analysis was performed using an Agilent 1200 instrument equipped with photodiode array detector with detection at 222 nm on a Vydac C_{18} at a flow rate of 0.2 ml/min. Samples' identity was confirmed by ESI-MS (Calculated mass for F-hIAPP17–29: C78H101N18O25 1689.71. Observed $[M+H]^+$: 1690.53, $[M+2H]^{2+}$: 845,47. Calculated mass for F-rIAPP17–29: C80H110N18O24 1706.80. Observed $[M+H]^+$: 1707.53, $[M+2H]^{2+}$: 853.73).

4.3. Sample preparation

To remove any pre-existing aggregated form, especially for hIAPP1–37 or hIAPP17–29, all peptide samples were subjected to an appropriated disaggregating procedure before carrying out each experiment. The following protocol was applied: samples were dissolved in 1,1,1,3,3,3-hexa-fluoro-2-propanol (HFIP) at a concentration of 1 mg/1 ml and incubated at 37 °C for 1 h. HFIP was removed by gentle streaming of argon, the peptide film was dissolved again in 1 ml HFIP, frozen at −30 °C for 4–5 h, then lyophilized overnight. The lyophilized samples were then dissolved in 2 mM phosphate buffer pH 7.0 (or 2 mM phosphate buffer pH 7.0 containing 200 μM POPC) to a concentration of 20 μM, ready for the CD, DLS or Th-T measurements. In the case of biological experiments the lyophilized sample were dissolved in Dimethylsulfoxide (DMSO) at a 5 mM concentration stock solution.

4.4. Preparation of model membranes

Model membranes were prepared by drying lipid solutions in $CHCl_3$ with a stream of dry nitrogen gas. The resulting lipid film was then fully evaporated under high vacuum to dryness in a round-bottomed flask. POPC multilamellar vesicles (MLVs) were obtained by hydrating the resulting lipid film with an appropriate amount of buffer (2 mM phosphate buffer pH 7.0) and dispersed by vigorous stirring at room temperature. The final concentration of lipids was 200 μM. Large Unilamellar Vesicles (LUVs), were obtained by extrusion of the MLVs through polycarbonate filters (pore size ~ 100 nm; Nuclepore, Pleasanton, CA) mounted in a mini-extruder (Avestin, Ottawa, ON, Canada) fitted with two 0.5 ml Hamilton gastight syringes (Hamilton, Reno, NV). Samples were typically subjected to more than 20 passes through two filters in tandem as recommended elsewhere [64,65].

4.5. Circular dichroism (CD) spectroscopy

The CD spectra were obtained at 37 °C under a constant flow of N2 on a Jasco J-810 spectropolarimeter equipped with a Peltier thermoelectric type temperature control system. Experimental measurements were conducted in 2 mM phosphate buffer pH 7.0 using 1 cm or 0.1 cm path length cuvettes. The CD spectra were recorded in the UV region (190–260 nm) with peptide concentration of 20 μM. The CD spectra were acquired every 20 min over an experimental time course of 21 h. In the case of hIAPP1–37 CD monitoring was prolonged up to 40 h. CD intensities are expressed as mean residue ellipticity [θ](deg cm^2 $dmol^{-1}$).

4.6. Dynamic Light Scattering (DLS)

DLS experiments were performed by using a polarized He–Ne laser (632.8 nm) with a power of 35 mW as source impinging to the sample; the collected scattered light was sent to a Malvern 4700 sub-micrometre particle analyzer system to obtain the scattered intensity autocorrelation function, $g1(\tau)$ [66]. The solutions were thermostated at 37 ± 0.02 °C. The cumulant analysis method was used to extract from $g1(\tau)$ the diffusion coefficient, D, of particles in solution. The hydrodynamic radius was calculated through the Einstein–Stokes relation: $RH = kBT/(6\pi\eta D)$, where kB is the Boltzmann's constant, T the absolute temperature and η the solvent viscosity [67]. The size distribution of the aggregates was obtained by the Laplace inversion of the scattered intensity autocorrelation function [66].

4.7. Thioflavin-T (Th-T) assay

Fluorescence emission spectra of Th-T undergo a red shift upon incorporation into β-sheet amyloid structures. A VarioSkan Flash from Thermo Scientific fluorescence 96-well plate reader was used for the Th-T measurements. To minimize evaporation effects the wells were sealed by a transparent heat-resistant plastic film. Readings were taken every 10 min, after weak shaking for 10 s, over a window of time of 1400 min. Fluorescence excitation was at 440 nm and emission detected at 480 nm. To minimize errors during sample preparation we have freeze-dried the 20 μM hIAPP1–37, hIAPP17–29, rIAPP1–37 and rIAPP17–29 solutions (prepared according to the above described sample preparation protocol) directly in the well plate. All Th-T experiments were carried out at pH 7.0, at 37 °C and in 2 mM Phosphate buffer. In all buffers the Th-T concentration was 60 μM.

4.8. Cell culture

Rat insulinoma RIN-M and INS-1 cells (from EACC) were cultured in 5% CO_2 in RPMI 1640 (Invitrogen) supplemented with 10% FBS (Invitrogen), 1% penicillin/streptomycin (Invitrogen), and INS-1 were supplemented with 20% of a stock solution containing 5 mM HEPES, 100 mM L-glutamine, 100 mM sodium pyruvate, and 2.5 mM 2-mercaptoethanol (all from Sigma). Once the cells reached 95% confluence, they were split (using 0.25% trypsin-EDTA; Invitrogen) into fractions and propagated or used in experiments. Cells were passage weekly. Passages 10–30 were used for all the experiments.

4.9. Cell viability assays

Cell viability was estimated by using the MTT assay (3-(4,5-dimethylthiazol-2-yl)-2,5-diphenyltetrazolium bromide) [68], TMRM (Tetramethylrhodamine methyl ester) uptake and PI staining. MTT determination involves reduction of the tetrazolium salt MTT to purple formazan crystals in living cells. For this assay, 2×10^4 cells/well were plated in 200 μl medium in 96-well plates (Falcon; BD Biosciences). After culturing for 24 h, the medium was replaced with medium containing the desired peptides concentration and the incubation was continued for 48–62 h. The range of concentrations was chosen considering the values commonly adopted across the field to generate amylin oligomers and aggregates toxic to cells. Thereafter, for each well, the medium was replaced with fresh medium containing 0.5 mg/ml MTT (Sigma) and incubated at 37 °C for 3 h. The formazan crystals produced by

MTT reduction were dissolved by using DMSO (Sigma), and the absorbance (λ 569 nm) was measured on a Varioskan flash spectral scanning multimode microplate reader (Thermo Scientific), with a reference λ of 670 nm to subtract background. TMRM accumulates in active mitochondria due its positive charge whereby the reduction of $\Delta\Psi_m$ leads to the release of TMRM. After treatments adherent cells were washed with PBS and then incubated for 30 min at 37 °C with Krebs Ringer Buffered Saline (130 mM NaCl, 3.6 mM KCl, 10 mM HEPES, 2 mM $NaHCO_3$, 0.5 mM NaH_2PO_4, 0.5 mM $MgCl_2$, 1.5 mM $CaCl_2$, 4.5 g/l glucose, pH 7.42) supplemented with 200 nM TMRM and 20 μM Verapamil (a multi drug-resistant pump inhibitor) (Sigma). Cells were then detached by short treatment with trypsin–EDTA, re-suspended in the above buffer, supplemented with 1% FCS to neutralize the trypsin, and immediately analyzed on a CyFlow® ML flow cytometer (Partec) in FL3 log mode. The $\Delta\Psi_m$ of RIN-M cells was estimated by gating cells with high red values (TMRM) characteristic of polarised mitochondria. The gate value for polarised mitochondria was fixed by using 1 μM of the uncoupling agent FCCP as depolarization control. Total levels of cellular ATP used to assess cell viability, cell proliferation and cytotoxicity was quantified by measuring the light produced through its reaction with the enzyme Luciferase by using the Luminescent ATP Detection assay kit (Abcam). RIN-M cells were pleated in a 96 well plated, exposed for 5 h to the desired concentration of peptides and processed according to the manufacturer instruction. A VarioSkan Flash from Thermo Scientific fluorescence 96-well plate reader was used for the lecture of Luciferase signal. PI is not membrane permeant and generally it is excluded from viable cells; then it is commonly used for identifying dead cells in a population. At the end of each treatment RIN-M cells were loaded with 0.5 μM PI for 20 min at 37 °C. The percentage of cells stained with PI was measured by flow cytometry (CyFlow® ML-Partec) on FL3 log mode.

4.10. Imaging and confocal microscopy

Cells were plated in 35-mm glass-bottom Willco Wells cell culture dishes (Willco Wells). After culturing for 24 h, the medium was replaced with phenol red-free medium containing the desired concentration of IAPP peptides and incubated over the time. When required, 30 min prior to imaging, the medium was replaced with fresh medium containing 50 nM of the mitochondrial markers MitoTracker Deep Red or Lysotracker red (Molecular Probes). Finally, immediately prior to imaging, the medium was once again replaced with fresh medium to remove any extracellular markers. Ten random fields for each well were imaged, with each treatment repeated twice in three separate experiments. Imaging was carried out on an Olympus FV1000 confocal microscope, using a 63 Plan-Apo/1.4-NA oil-immersion objective. Standard three confocal channels (3 Photomultiplier detectors) acquisitions were made by using the following lasers mounted on a laser combiner: Multi-line Argon laser (457 nm, 488 nm, 515 nm), total 30 mW HeNe-Green laser (543 nm), 1.5 mW HeNe-Red laser (633 nm), 10 mW. Single optical sections (0.42 μm z axis) through the middle of the cells were acquired for each field. The pinhole was adjusted to keep the same size of z-optical sections for all analysis carried out. Sequential mode imaging was performed to ensure that there was no crosstalk between the channels. The extent of amylin binding and internalization in rat insulinoma cells was quantified using both the FV1000 (release 2.0). The fluorescence intensity of each cell was measured in a region of interest (ROI) delimitating a single cell, by calculating the mean fluorescence intensity (MFI) at the emission wavelength established. The Pearson co-localization coefficient (R) calculated by using the Olympus FV1000 co-localization software (release 2.0) was employed to estimate the co-localization of mitochondrial F-IAPP peptides and the mitochondrial marker MitoTracker.

4.11. Indirect immunofluorescence of adherent cells

Cells were exposed to 25 μM of freshly prepared IAPP peptides for around 6 h, washed repeatedly with PBS to remove non-bound monomers and oligomers, and then fixed in 3.7% paraformaldehyde for 30 min at room temperature. Fixed cells were permeabilized using 0.3% Triton X-100 and unspecific binding was blocked by 30 min of incubation in 0.2% gelatine in PBS. Membrane-bound and internalized soluble amylin monomers and oligomers were detected by incubating overnight cells with rabbit anti-amylin antibody (1:100, SC-20936 Santa Cruz) or rabbit anti-oligomer A11 antibody (1:200, AHB0052 Invitrogen) [37]. After washes in PBS, cells were exposed for 1 h at room temperature to the respective anti-rabbit secondary antibody conjugated with AlexaFluor 546 or AlexaFluor 488, mounted with the ProLong Gold antifade mounting medium (Invitrogen) or with DAPI-Fuoromont G (Southern Biotechnology) and examined under a FV1000 confocal microscope using the Fluoview Olympus image software (release 2.0).

4.12. Detection of ROS

Intracellular ROS were measured using dichlorofluorescein diacetate (DCFH, Invitrogen), an oxidation-sensitive fluorescent probe. This test is based on the principle that endogenous esterases hydrolyse DCFH, trapping free DCF inside the cells. ROS, predominantly hydroperoxides, convert non-fluorescent DCF into highly fluorescent DCF. After incubation with IAPP peptides, cells were loaded with 20 μM DCFH for 30 min at 37 °C in the dark. Cells were then analyzed on a CyFlow® ML flow cytometer (Partec) measuring the fluorescence emission in FL1 log mode.

4.13. Flow cytometry

20.000 cells per sample were analyzed using a CyFlow® ML flow cytometer (Partec) system equipped with three laser sources and 10 optical parameters with dedicated filter setting and a high numerical aperture microscope objective (50× NA 0.82) for the detection of different scatter and fluorescence signals. The cells were excited by an air-cooled argon 488 nm laser and then the signal from DCFH and carboxyfluorescein was read on FL1 detector while the signal from TMRM and PI on FL3 detector. Data obtained were acquired, gated, compensated, and analysed using the FlowMax software (Partec). Each experiment was repeated at least twice in triplicate.

4.14. Statistical analysis

Values are expressed as mean ± SEM. Statistical analysis was performed by one-way ANOVA with Tukey's post hoc test. A $P < 0.05$ was taken as significant. All data from flow cytometry were representative for at least two sets of independent experiments performed in triplicate and based on at least 20.000 events for each group. The difference among different groups was examined using χ^2 test. A P value below 0.001 was considered to be significant.

5. Conclusions

A conformational spectroscopic study was carried out together with an investigation of the peptide toxicity towards β-cell lines in vitro. According to a widely accepted model, oligomers from full-length hIAPP may be involved in cytotoxicity. In this work, the shorter hIAPP17–29 reproduced similar cytotoxic behaviour just

like the parent full-length hIAPP1–37, but no conformational transitions toward β-sheet structure was observed in vitro by the shorter peptide fragment. Our results also indicate that rIAPP mediated β-cell toxicity can occur despite no sign of progression towards amyloid forms and this event imposes a re-evaluation of the experimental results available in this field to date.

Acknowledgements

Authors thank MIUR FIRB-MERIT RBNE08HWLZ and PRIN 2009 WCNS5C for financial support. Thanks are also due to Dr. V. Villari and N. Micali IPCF-CNR Messina (Italy) for carrying out the DLS measurements and helpful discussions.

Appendix A. Supplementary data

Supplementary data related to this article can be found at http://dx.doi.org/10.1016/j.ejmech.2014.05.038.

References

[1] J.D. Sipe, Amyloidosis, Crit. Rev. Clin. Lab. Sci. 31 (1994) 325–354.
[2] F. Chiti, C.M. Dobson, Protein misfolding, functional amyloid, and human disease, Annu. Rev. Biochem. 75 (2006) 333–336.
[3] A. Clark, C.A. Wells, I.D. Buley, J.K. Cruickshank, R.I. Vanhagan, D.R. Matthews, G.J.S. Cooper, R.R. Holmann, R.C. Turner, Islet amyloid, increased A-cells, reduced B-cells and exocrine fibrosis: quantitative changes in the pancreas in type 2 diabetes, Diab. Res. 9 (1988) 151–159.
[4] M.R. Hayden, S.C. Tyagi, M.M. Kerklo, M.R. Nicolls, Type 2 diabetes mellitus as a conformational disease, JOP 6 (2005) 287–302.
[5] P. Westermark, E. Wilander, G.T. Westermark, K.H. Johnson, Islet amyloid polypeptide-like immunoreactivity in the islet B cells of Type 2 (non-insulin-dependent) diabetic and non-diabetic individuals, Diabetologia 30 (1987) 887–892.
[6] P. Westermark, A. Andersson, G.T. Westermark, Islet amyloid polypeptide, islet amyloid, and diabetes mellitus, Physiol. Rev. 91 (2011) 795–826.
[7] G. Liu, A. Prabhakar, D. Aucoin, M. Simon, S. Sparks, K.J. Robbins, A. Sheen, S.A. Petty, N. Lazo, Mechanistic studies of peptide self-assembly: transient α-helices to stable β-sheets, J. Am. Chem. Soc. 132 (2010) 18223–18232.
[8] A. Kapurniotu, Amyloidogenicity and cytotoxicity of islet amyloid polypeptide, Biopolymers 60 (2001) 438–459.
[9] R. Kayed, J. Bernhagen, N. Greenfield, K. Sweimeh, H. Brunner, W. Voelter, A. Kapurniotu, Conformational transitions of islet amyloid polypeptide (IAPP) in amyloid formation in vitro, J. Mol. Biol. 287 (1999) 781–796.
[10] M.D. Kirkitadze, G. Bitan, D.B. Teplow, Paradigm shifts in Alzheimer's disease and other neurodegenerative disorders: the emerging role of oligomeric assemblies, J. Neurosci. Res. 69 (2002) 567–577.
[11] D.M. Walsh, D.J. Selkoe, Oligomers on the brain: the emerging role of soluble protein aggregates in neurodegeneration, Protein Pept. Lett. 11 (2004) 213–228.
[12] L. Haataja, T. Gurlo, C.J. Huang, P.C. Butler, Islet amyloid in type 2 diabetes, and the toxic oligomer hypothesis, Endocr. Rev. 29 (2008) 303–316.
[13] T. Gurlo, S. Ryazantsev, C.J. Huang, M.W. Yeh, H.A. Reber, O.J. Hines, T.D. O'Brien, C.G. Glabe, P.C. Butler, Evidence for proteotoxicity in beta cells in type 2 diabetes: toxic islet amyloid polypeptide oligomers form intracellularly in the secretory pathway, Am. J. Pathol. 176 (2010) 861–869.
[14] a) J.R. Brender, S. Salamekh, A. Ramamoorthy, Membrane disruption and early events in the aggregation of the diabetes related peptide IAPP from a molecular perspective, Acc. Chem. Res. 45 (2012) 454–462;
b) M.F. Engel, Membrane permeabilization by islet amyloid polypeptide, Chem. Phys. Lipids 160 (2009) 1–10.
[15] S. Zhang, J. Liu, E.L. Saafi, G.J. Cooper, Induction of apoptosis by human amylin in RINm5F islet beta-cells is associated with enhanced expression of p53 and p21WAF1/CIP1, FEBS Lett. 455 (1999) 315–320.
[16] S. Zraika, R.L. Hull, J. Udayasankar, K. Aston-Mourney, S.L. Subramanian, R. Kisilevsky, W.A. Szarek, S.E. Kahn, Oxidative stress is induced by islet amyloid formation and time-dependently mediates amyloid-induced beta cell apoptosis, Diabetologia 52 (2009) 626–635.
[17] S.L. Subramanian, R.L. Hull, S. Zraika, K. Aston-Mourney, J. Udayasankar, S.E. Kahn, cJUN N-terminal kinase (JNK) activation mediates islet amyloid-induced beta cell apoptosis in cultured human islet amyloid polypeptide transgenic mouse islets, Diabetologia 55 (2012) 166–174.
[18] N. Sánchez de Groot, I. Pallarés, F.X. Avilés, J. Vendrell, S. Ventura, Prediction of "hot spots" of aggregation in disease-linked polypeptides, BMC Struct. Biol. 5 (2005) 18.
[19] A. Abedini, D.P. Raleigh, Destabilization of human IAPP amyloid fibrils by proline mutations outside of the putative amyloidogenic domain: is there a critical amyloidogenic domain in human IAPP? J. Mol. Biol. 355 (2006) 274–281.
[20] A. Fox, T. Snollaerts, C.E. Casanova, A. Calciano, L.A. Nogaj, D.A. Moffet, Selection for nonamyloidogenic mutants of islet amyloid polypeptide (IAPP) identifies an extended region for amyloidogenicity, Biochemistry 49 (2010) 7783–7789.
[21] E.T.A.S. Jaikaran, C.E. Higham, L.C. Serpell, J. Zurdo, M. Gross, A. Clark, P.E. Fraser, Identification of a novel human islet amyloid polypeptide beta-sheet domain and factors influencing fibrillogenesis, J. Mol. Biol. 308 (2001) 515–525.
[22] R. Azriel, E. Gazit, Analysis of the minimal amyloid-forming fragment of the islet amyloid polypeptide. An experimental support for the key role of the phenylalanine residue in amyloid formation, J. Biol. Chem. 276 (2001) 34156–34161.
[23] K. Tenidis, M. Waldner, J. Bernhagen, W. Fischle, M. Bergmann, M. Weber, M.L. Merkle, W. Voelter, H. Brunner, A. Kapurniotu, Identification of a penta- and hexapeptide of islet amyloid polypeptide (IAPP) with amyloidogenic and cytotoxic properties, J. Mol. Biol. 295 (2000) 1055–1071.
[24] L.A. Scrocchi, Y. Chen, K.S. Waschu, F. Wang, S. Cheung, A.A. Darabie, J. McLaurin, P.E. Fraser, Design of peptide-based inhibitors of human islet amyloid polypeptide fibrillogenesis, J. Mol. Biol. 318 (2002) 697–706.
[25] G. Pappalardo, D. Milardi, A. Magrì, F. Attanasio, G. Impellizzeri, C. La Rosa, D. Grasso, E. Rizzarelli, Environmental factors differently affect human and rat IAPP: conformational preferences and membrane interactions of IAPP 17-29 peptide derivates, Chem. Eur. J. 13 (2007) 10204–10215.
[26] A. Mazzaglia, N. Micali, L.M. Scolaro, F. Attanasio, A. Magrí, G. Pappalardo, V. Villari, Aggregation properties of the peptide fragments derived from the 17–29 region of the human and rat IAPP: a comparative study with two PEG-conjugated variants of the human sequence, J. Phys. Chem. B 114 (2010) 705–713.
[27] A.V. Matveyenco, P.C. Butler, Islet amyloid polypeptide (IAPP) transgenic rodents as models for type 2 diabetes, ILAR J. 47 (2006) 225–233.
[28] P. Cao, P. Marek, H. Noor, V. Patsalo, L.H. Tu, H. Wang, A. Abedini, D.P. Raleigh, Islet amyloid: from fundamental biophysics to mechanisms of cytotoxicity, FEBS Lett. 587 (2013) 1106–1118.
[29] A. Perczel, M. Hallosi, in: G.D. Fasman (Ed.), Circular Dichroism and the Conformational Analysis of Biomolecules, Plenum Press, New York, 1996, pp. 285–380.
[30] N. Micali, V. Villari, G.M. Consoli, F. Cunsolo, C. Geraci, Vesicle-to-micelle transition in aqueous solutions of amphiphilic calixarene derivatives, Phys. Rev. E. Stat. Nonlin. Soft Matter Phys. 73 (2006) n° 051904.
[31] J. Janson, R.H. Ashley, D. Harrison, S. McIntyre, P.C. Butler, The mechanism of islet amyloid polypeptide toxicity is membrane disruption by intermediate-sized toxic amyloid particles, Diabetes 48 (1999) 491–498.
[32] S. Janciauskiene, B. Ahrén, Different sensitivity to the cytotoxic action of IAPP fibrils in two insulin-producing cell lines, HIT-T15 and RINm5F cells, Biochem. Biophys. Res. Commun. 251 (1998) 888–893.
[33] M. Magzoub, A.D. Miranker, Concentration-dependent transitions govern the subcellular localization of islet amyloid polypeptide, FASEB J. 26 (2012) 1228–1238.
[34] J.M. Dypbukt, M. Ankarcrona, M. Burkitt, A. Sjöholm, K. Ström, S. Orrenius, P. Nicotera, Different prooxidant levels stimulate growth, trigger apoptosis, or produce necrosis of insulin-secreting RINm5F cells. The role of intracellular polyamines, J. Biol. Chem. 269 (1994) 30553–30560.
[35] B. Konarkowska, J.F. Aitken, J. Kistler, S. Zhang, G.J. Cooper, Thiol reducing compounds prevent human amylin-evoked cytotoxicity, FEBS J. 272 (2005) 4949–4959.
[36] M. Wakabayashi, K. Matsuzaki, Ganglioside-induced amyloid formation by human islet amyloid polypeptide in lipid rafts, FEBS Lett. 583 (2009) 2854–2858.
[37] R. Kayed, E. Head, J.L. Thompson, T.M. McIntire, S.C. Milton, C.W. Cotman, C.G. Glabe, Common structure of soluble amyloid oligomers implies common mechanism of pathogenesis, Science 300 (2003) 486–489.
[38] P. Westermark, U. Engström, K.H. Jonshon, G.T. Westermark, C. Betsholtz, Islet amyloid polypeptide: pinpointing amino acid residues linked to amyloid fibril formation, Proc. Natl. Acad. Sci. U. S. A. 87 (1990) 5036–5040.
[39] A.D. Abedini, P. Raleigh, The role of His-18 in amyloid formation by human islet amyloid polypeptide, Biochemistry 44 (2005) 16284–16291.
[40] K. Yanagi, M. Ashizaki, H. Yagi, K. Sakurai, Y.H. Lee, Y. Goto, Hexafluoroisopropanol induces amyloid fibrils of islet amyloid polypeptide by enhancing both hydrophobic and electrostatic interactions, J. Biol. Chem. 286 (2011) 23959–23966.
[41] H. Naiki, K. Higuchi, M. Hosokawa, T. Takeda, Fluorometric determination of amyloid fibrils in vitro using the fluorescent dye, thioflavin T1, Anal. Biochem 177 (1989) 244–249.
[42] H. LeVine 3rd, Thioflavine T interaction with synthetic Alzheimer's disease beta-amyloid peptides: detection of amyloid aggregation in solution, Protein Sci. 2 (1993) 404–410.
[43] K.J. Potter, L.A. Scrocchi, G.L. Warnock, Z. Ao, M.A. Younker, L. Rosenberg, M. Lipsett, C.B. Verchere, P.E. Fraser, Amyloid inhibitors enhance survival of cultured human islets, Biochim. Biophys. Acta 1790 (2009) 566–574.
[44] C.E. Higham, E.T. Jaikaran, P.E. Fraser, M. Gross, A. Clark, Preparation of synthetic human islet amyloid polypeptide (IAPP) in a stable conformation to enable study of conversion to amyloid-like fibrils, FEBS Lett. 470 (2000) 55–60.

[45] X. Zhang, B. Cheng, H. Gong, C. Li, H. Chen, L. Zheng, K. Huang, Porcine islet amyloid polypeptide fragments are refractory to amyloid formation, FEBS Lett. 585 (2011) 71–77.
[46] P. Cao, L.H. Tu, A. Abedini, O. Levsh, R. Akter, V. Patsalo, A.M. Schmidt, D.P. Raleigh, Sensitivity of amyloid formation by human islet amyloid polypeptide to mutations at residue 20, J. Mol. Biol. 421 (2012) 282–295.
[47] N.G.N. Milton, J.R. Harris, Fibril formation and toxicity of the non-amyloidogenic rat amylin peptide, Micron 44 (2013) 246–253.
[48] Y.A. Lim, L.M. Ittner, Y.L. Lim, J. Götz, Human but not rat amylin shares neurotoxic properties with Abeta42 in long-term hippocampal and cortical cultures, FEBS Lett. 582 (2008) 2188–2194.
[49] S. Luca, W.M. Yau, R. Leapman, R. Tycko, Peptide conformation and supramolecular organization in amylin fibrils: constraints from solid-state NMR, Biochemistry 46 (2007) 13505–13522.
[50] S. Salamekh, J.R. Brender, S.J. Hyung, R.P. Nanga, S. Vivekanandan, B.T. Ruotolo, A. Ramamoorthy, A two-site mechanism for the inhibition of IAPP amyloidogenesis by zinc, J. Mol. Biol. 410 (2011) 294–306.
[51] J.Z. Bai, E.L. Saafi, S. Zhang, G.J. Cooper, Role of Ca^{2+} in apoptosis evoked by human amylin in pancreatic islet beta-cells, Biochem. J. 343 (1999) 53–61.
[52] S. Trikha, A.M. Jeremic, Clustering and internalization of toxic amylin oligomers in pancreatic cells require plasma membrane cholesterol, J. Biol. Chem. 286 (2011) 36086–36097.
[53] J.F. Paulsson, S.W. Schultz, M. Köhler, I. Leibiger, P.O. Berggren, G.T. Westermark, Real-time monitoring of apoptosis by caspase-3-like protease induced FRET reduction triggered by amyloid aggregation, Exp. Diabetes Res. (2008) 865850.
[54] A. Abedini, A.M. Schmidt, Mechanisms of islet amyloidosis toxicity in type 2 diabetes, FEBS Lett. 587 (2013) 1119–1127.
[55] A. Nath, A.D. Miranker, E. Rhoades, A membrane-bound antiparallel dimer of rat islet amyloid polypeptide, Angew. Chem. Int. Ed. Engl. 50 (2011) 10859–10862.
[56] N.B. Last, E. Rhoades, A.D. Miranker, Islet amyloid polypeptide demonstrates a persistent capacity to disrupt membrane integrity, Proc. Natl. Acad. Sci. U. S. A. 108 (2011) 9460–9465.
[57] T.A. Mirzabekov, M.C. Lin, B.L. Kagan, Pore formation by the cytotoxic islet amyloid peptide amylin, J. Biol. Chem. 271 (1996) 1988–1992.
[58] J.D. Knight, J.A. Hebda, A.D. Miranker, Conserved and cooperative assembly of membrane-bound alpha-helical states of islet amyloid polypeptide, Biochemistry 45 (2006) 9496–9508.
[59] M.F.M. Engel, L. Khemtemourian, C.C. Kleijer, H.J.D. Meeldijk, J. Jacobs, A.J. Verkleij, B. de Kruijff, J.A. Killian, J.W. Höppener, Membrane damage by human islet amyloid polypeptide through fibril growth at the membrane, Proc. Natl. Acad. Sci. U. S. A. 105 (2008) 6033–6038.
[60] P. Li, D. Nijhawan, I. Budihardjo, S.M. Srinivasula, M. Ahmad, E.S. Alnemri, X. Wang, Cytochrome c and dATP-dependent formation of Apaf-1/caspase-9 complex initiates an apoptotic protease cascade, Cell 91 (1997) 479–489.
[61] P. Gubellini, B. Picconi, M. Di Filippo, P. Calabresi, Downstream mechanisms triggered by mitochondrial dysfunction in the basal ganglia: from experimental models to neurodegenerative diseases, Biochim. Biophys. Acta 1802 (2010) 151–161.
[62] M. Stefani, C.M. Dobson, Protein aggregation and aggregate toxicity: new insights into protein folding, misfolding diseases and biological evolution, J. Mol. Med. 81 (2003) 678–699.
[63] M. Bucciantini, G. Calloni, F. Chiti, L. Formigli, D. Nosi, C.M. Dobson, M. Stefani, Prefibrillar amyloid protein aggregates share common features of cytotoxicity, J. Biol. Chem. 279 (2004) 31374–31382.
[64] M.F.M. Sciacca, D. Milardi, G.M.L. Messina, G. Marletta, J.R. Brender, Cations as switches of amyloid-mediated membrane disruption mechanisms: calcium and IAPP, Biophys. J. 104 (2013) 173–184.
[65] D. Milardi, M.F.M. Sciacca, M. Pappalardo, D.M. Grasso, C. La Rosa, The role of aromatic side-chains in amyloid growth and membrane interaction of the islet amyloid polypeptide fragment LANFLVH, Eur. Biophys. J. 40 (2011) 1–12.
[66] V. Villari, N. Micali, Light scattering as spectroscopic tool for the study of disperse systems useful in pharmaceutical sciences, J. Pharm. Sci. 97 (2008) 1703–1730.
[67] B. Chu, Laser Light Scattering-basic Principle and Practice, San Diego Academic, 1991.
[68] T.J. Mosmann, Rapid colorimetric assay for cellular growth and survival: application to proliferation and cytotoxicity assays, Immunol. Methods 65 (1983) 55–63.